Adsorption 10: 111–128, 2004

Diffusion Mechanism of Carbon Dioxide in Zeolite 4A and CaX Pellets

HYUNGWOONG AHN* AND JONG-HO MOON
Department of Chemical Engineering, Yonsei University, 134 Shinchon-dong, Seodaemun-gu, Seoul, 120-749, Korea

SANG-HOON HYUN
Department of Ceramic Engineering, Yonsei University, 134 Shinchon-dong, Seodaemun-gu, Seoul, 120-749, Korea

CHANG-HA LEE†
Department of Chemical Engineering, Yonsei University, 134 Shinchon-dong, Seodaemun-gu, Seoul, 120-749, Korea
leech@yonsei.ac.kr

Received February 26, 2003; Revised January 13, 2004; Accepted March 29, 2004

Abstract. The adsorption kinetics and equilibria of CO_2 in commercial zeolite 4A and CaX pellets were theoretically and experimentally studied by a gravimetric method in the range of 273–313 K and 0.0–0.8 atm. The diffusion mechanism of an adsorbate into a pellet is composed of micropore and macropore diffusion due to the bidisperse structure of the pellet. When one diffusion mechanism played a more important role than the other in determining the overall diffusion rate, the diffusion rate was estimated by the nonisothermal monodisperse diffusion model (NMDM). However, when the combined effects of both mechanisms controlled the overall adsorption kinetics, the experimental uptake was analyzed by the nonisothermal bidisperse diffusion model (NBDM). The CO_2 diffusion in zeolite 4A pellets was controlled by micropore diffusion within the experimental pressure and temperature ranges. However, both macropore and micropore diffusion contributed to CO_2 diffusion in the zeolite CaX pellet. The overall CO_2 diffusion rate in zeolite CaX became faster as pressure increased mainly due to its highly favorable isotherm in the zeolite CaX. The micropore diffusion time constant of CO_2 in the zeolite CaX pellet was approximately one hundred times greater than that in the zeolite 4A pellet. In addition, the activation energy of micropore diffusion of CO_2 diffusion in the zeolite CaX pellet was smaller than that in the zeolite 4A pellet. In this study, the dimensionless parameter, γ, indicating the relative importance of macropore and micropore diffusion, was modified to consider non-zero coverage as an initial condition for each step in the gravimetric method. When γ is greater than 100, the overall adsorption rate is controlled by macropore diffusion. However, in cases where γ is less than 0.1, micropore diffusion is the dominant mechanism in the overall adsorption rate. In the case of a system with γ between these values, both macropore and micropore diffusion contributed to the overall diffusion rate.

Keywords: adsorption, diffusion, zeolites, kinetics, carbon dioxide, bidisperse

*Present address: Department of Chemical Engineering, University College London, Torrington Place, London WC1E 7JE, UK.
†To whom correspondence should be addressed.

Introduction

Pelletized zeolites have an explicit bidisperse distribution of pores because they are produced by the consolidation of crystals with the binders. In the zeolite pellet, the following diffusion resistances play a key role in the adsorption kinetics: micropore diffusion, macropore diffusion, external film mass transfer and heat transfer resistance. In general, the diffusion rates of adsorption and desorption in the gas phase depend on intraparticle diffusion rather than external film resistance (Yucel and Ruthven, 1980a; Ruthven et al., 1980). And it is assumed that there is no radial temperature distribution in the pellet and the dominant heat transfer resistance is in the external stagnant film of the particle (Gray and Do, 1991).

The ratio of the micropore size to the kinetic diameter of diffusing molecules is normally regarded as an important factor affecting the diffusion rate. While the diffusion rate in zeolite 5A crystal is much faster than that in zeolite 4A crystal, the activation energy of micropore diffusion in zeolite 5A crystal is smaller than that in zeolite 4A crystal (Yucel and Ruthven, 1980b). Furthermore, it was pointed out that the low diffusion coefficient meant the great resistance of the diffusion as well as the higher energy barriers for molecules (Ma and Mancel, 1972).

The larger the size of the crystal becomes, the adsorption kinetics become closer to isothermal behavior because the nonisothermality does not depend on the diffusivity, D, but rather the diffusion time constant, D/R^2 (Yucel and Ruthven, 1980b; Ruthven et al., 1980). Ruthven and co-workers studied the diffusion mechanisms of CO_2 in zeolite 4A and 5A crystals by using two different crystal sizes and varying amounts of adsorbents (Yucel and Ruthven, 1980b; Ruthven et al., 1980). The CO_2 diffusion in zeolite 4A crystal was controlled by intracrystalline diffusion and resembled isothermal behavior, while the CO_2 diffusion in zeolite 5A crystal showed nonisothermal behavior and was controlled by external heat transfer. They also showed that a similar value of heat transfer coefficient, h, could be obtained from the nonlinear regression of the experimental uptake curve regardless of pressure range if the adsorbent beds with similar crystal size and bed configuration were used.

The adsorption rates in crystal and pellet have been measured by a gravimetric method, ZLC, chromatography, frequency response, and NMR (Ruthven and Xu, 1993; Yucel and Ruthven, 1980b; Ruthven, 1993). Meanwhile, the chromatographic method has been used for the rate measurement in the commercial zeolite pellet (Haq and Ruthven, 1986a, 1986b). The theoretical analysis of the chromatographic method depended on the moment method with an axial dispersion and an assumption of isothermal adsorption. However, the isothermal assumption was suitable only for the adsorption at a high temperature and a low adsorbate concentration (Ma and Mancel, 1972). Since the CO_2 adsorptions in zeolite 4A and 5A pellets have relatively great heat of adsorption, it is hard to assume that it would be isothermal at the ambient temperature. Therefore, the reported kinetic information on the CO_2 diffusions in zeolite 4A and 5A pellets was limited within the very high temperature range (more than 500 K) (Haq and Ruthven, 1986a, 1986b).

Recently, it is remarkable that the ZLC technique has been applied to the measurement of adsorption rate from the zeolite crystal to the zeolite pellet. Brandani (1996) and Silva and Rodrigues (1996) suggested the analytical solution for the ZLC desorption curve in the biporous adsorbent like zeolite pellet. Furthermore, a nonisothermal simple model was developed for the analysis of ZLC experiments considering the heat effect (Silva et al., 2001). In addition, adsorption rates of various hydrocarbons in several zeolite pellets were measured using a ZLC technique and dominant diffusion mechanisms were elucidated in the systems (Silva et al., 1997; Da Silva et al., 1999).

Ruthven and Xu (1993) pointed out that the macropore diffusion resistance was dominant in the N_2 diffusion in the commercial zeolite 5A pellet by between the apparent diffusion time constants in pellets of two different sizes. Recently, the macropore diffusion control of the N_2 diffusion in the zeolite 5A pellet was confirmed by Ahn et al. (2002). Furthermore, they presented the diffusion mechanisms of N_2 and CH_4 in zeolite 4A, 5A and CaX pellets by using the gravimetric method. It was also reported that the diffusion rate of CO_2 in the commercial zeolite 4A pellet was controlled by micropore diffusion (Haq and Ruthven, 1986a).

In this study, the diffusion mechanisms of CO_2 in commercial zeolite 4A and CaX pellets were compared theoretically and experimentally in the range of 0.0–0.8 atm and 273–313 K. The apparent diffusivity was obtained by matching the experimental uptake curves to nonisothermal monodisperse diffusion model (NMDM). From the comparison of the apparent diffusion time constants in pellets of two different sizes, it was possible to estimate which diffusion

mechanism would be more dominant. When both macropore and micropore diffusions contributed to overall diffusion rate, nonisothermal bidisperse diffusion model (NBDM) developed in this study was applied to the analysis of the uptake curve. The dimensionless parameter, γ, which expresses the relative importance of macropore and micropore diffusions in the zeolite pellet, was applied to the determination of dominant diffusion mechanism in a stepwise gravimetric method. By comparing the pre-determined dominant diffusion mechanism with the value of γ, the range of γ relating to each dominant diffusion mechanism was determined.

Mathematical Model

The general assumptions for NMDM and NBDM in pellet are as follows (Ruthven et al., 1980; Gray and Do, 1991):

- The resistance controlling the adsorption dynamics is not external film mass transfer but intraparticle diffusion such as macropore and micropore diffusions.
- Since the thermal conduction inside an individual particle and the heat transfer between the particles are very rapid, the only significant heat transfer resistance exists in the external film of the zeolite pellet.
- The crystal and the pellet are spherical.
- The equilibrium relations are linear in the experimental range of a differential pressure change.

Nonisothermal Monodisperse Diffusion Model (NMDM)

When either macropore or micropore diffusions dominates overall mass diffusion rate in pellet, the diffusivity can be estimated by nonlinear regression of analytical solution derived from NMDM (Ruthven et al., 1980; Ahn et al., 2002).

With the above-mentioned general assumptions, additional assumptions relating to NMDM are as follows:

- Only one of both micropore and macropore diffusion resistances is considered as overall diffusion resistance.
- The diffusivity in macropore or micropore is assumed constant in an uptake experiment because the pressure change at each experiment is very small.

When macropore diffusion resistance is negligible in overall diffusion rate, main diffusion resistance in pellet is related to mass transfer in crystal and heat transfer in external film. The analytical solution to governing equations of diffusion in crystal with a differential step change of concentration is as follows (Ruthven et al., 1980):

$$\frac{q-q_i}{q_e-q_i} = 1-\sum_{n=1}^{\infty}\frac{9\left[(p_n\cot p_n-1)/p_n^2\right]^2\exp\left(-p_n^2D_ct/R_c^2\right)}{1/\beta+3/2\left[p_n\cot p_n(p_n\cot p_n-1)/p_n^2+1\right]} \tag{1}$$

The corresponding temperature variation in crystal is as follows:

$$\frac{T_p-T_{pi}}{q_e-q_i}\left(\frac{\partial q_e}{\partial T}\right)_p = \sum_{n=1}^{\infty}\frac{-3\left[(p_n\cot p_n-1)/p_n^2\right]\exp\left(-p_n^2D_ct\,/\,R_c^2\right)}{1/\beta+3/2\left[p_n\cot p_n(p_n\cot p_n-1)/p_n^2+1\right]} \tag{2}$$

where p_n is given by the roots of the following equation.

$$3\beta(p_n\cot p_n-1)=p_n^2-\alpha \tag{3}$$

The parameters α and β are defined by

$$\alpha=\left(\frac{ha}{C_{ps}\rho_p}\right)\Big/\left(\frac{D_c}{R_c^2}\right),\quad \beta=\frac{\Delta H}{C_{ps}}\left(\frac{\partial q_e}{\partial T}\right)_p \tag{4}$$

The parameter α means the relative magnitude between heat transfer time constant and mass transfer time constant, and β indicates the magnitude of the heat effect in an uptake by means of both the heat of adsorption and the variation of equilibrium concentration with temperature. In the case of either $\alpha\to\infty$ or $\beta\to 0$, Eqs. (1)–(3) represent isothermal behavior. On the contrary, under the condition of $\alpha\to 0$ or $\beta\to\infty$, the diffusion behavior is controlled by the heat transfer rate rather than the mass transfer rate.

When macropore diffusion is more dominant as a rate-controlling step than micropore diffusion, the analytical solutions are the same as Eqs. (1)–(4) only if D_e is substituted for D_c and R_p for R_c (Ruthven et al., 1980).

In estimating the parameters in Eqs. (1)–(4), the number of parameters to be determined should be minimized. While the driving force of the diffusion was

concentration difference in the initial part of the uptake curve, the latter part of the uptake curve was totally controlled by the heat transfer between the adsorbent and the surrounding. Therefore, the limiting case of a complete heat transfer control was applied to the latter part of the uptake curve in order to determine the value of $ha/\rho C_{ps}$ in Eq. (4). Also, the value of β could be calculated from the slope of the isobar and the heat of adsorption. Finally, the value of D/R^2 could be found by matching the experimental uptake curve to Eq. (1).

Nonisothermal Bidisperse Diffusion Model (NBDM)

When both macropore and micropore diffusions contribute to overall mass transfer rate, the theoretical uptake curve can be obtained from NBDM. Gray and Do (1991) developed NBDM for the study of adsorption kinetics in the differential adsorption bed (DAB) packed with activated carbon. In general, while the surface diffusion in the macropore should be considered in studying the diffusion in the activated carbon, it could be neglected in the study of zeolitic diffusion (Do, 1998).

In addition to the above general assumptions, this model needs to include the following additional assumptions.

- The adsorption dynamics are affected by both macropore and micropore diffusions.
- The macropore and micropore diffusivities are independent of the adsorbate concentration within the differential pressure change, but they vary with temperature.
- The adsorbed amount in the entrance of the micropore is determined by the equilibrium adsorption amount at the adsorbate concentration in the macropore.

Given these assumptions, the mass balance for crystal is as follows:

$$\frac{\partial C_c}{\partial t} = D_c(T_p)\frac{1}{r_c^2}\frac{\partial}{\partial r_c}\left(r_c^2\frac{\partial C_c}{\partial r_c}\right) \tag{5}$$

The boundary conditions for Eq. (5) are given by

$$r_c = 0, \quad \frac{\partial C_c}{\partial r_c} = 0 \tag{6a}$$

$$r_c = R_c, \quad C_c = \frac{C_{cs}b(T_p)C_p}{1 + b(T_p)C_p} \tag{6b}$$

The mass balance for the pellet is represented by the following equation:

$$\varepsilon\frac{\partial C_p}{\partial t} + (1-\varepsilon)\frac{\partial \bar{C}_c}{\partial t} = \varepsilon D_p(T_p)\frac{1}{r_p^2}\frac{\partial}{\partial r_p}\left(r_p^2\frac{\partial C_p}{\partial r_p}\right) \tag{7}$$

The boundary conditions for Eq. (7) are as follows:

$$r_p = 0, \quad \frac{\partial C_p}{\partial r_p} = \frac{\partial \bar{C}_c}{\partial r_p} = 0 \tag{8a}$$

$$r_p = R_p, \quad \varepsilon D_p(T_p)\left.\frac{\partial C_p}{\partial r_p}\right|_{R_p} = k_m\left(C_b - C_p\big|_{R_p}\right) \tag{8b}$$

where $\bar{C}_c$ is the volume-average crystal concentration at the radial position in the pellet, r_p, and it is given by

$$\bar{C}_c = \frac{4\pi\int_0^{R_c} r_c^2 C_c\, dr_c}{4\pi\int_0^{R_c} r_c^2\, dr_c} \tag{9}$$

The heat balance over the pellet is as follows:

$$\rho_p C_{ps}\frac{dT_p}{dt} + \frac{3h(T_p - T_{pi})}{R_p} - \frac{3(1-\varepsilon)}{R_p^3}(-\Delta H) \times \int_0^{R_p}\frac{\partial \bar{C}_c}{\partial t}r_p^2 dr_p = 0 \tag{10}$$

where the accumulation term in the crystal can be equated with the flux at the surface of the crystal:

$$\frac{\partial \bar{C}_c}{\partial t} = D_c(T_p)\frac{3}{R_c}\left.\frac{\partial C_c}{\partial r_c}\right|_{R_c} \tag{11}$$

The value of the external film mass transfer coefficient, k_m, was calculated by using the postulation that Sherwood number is equal to 2 in stagnant gas phase (Wakao and Kaguei, 1982). The coupled partial differential equations were converted into the dimensionless form and were reduced to the ordinary differential equations by using orthogonal collocation technique. The detailed procedure of the numerical method is explained in the Appendix.

Dimensionless Parameter, γ

Do (1998) defines the dimensionless parameter, γ, to evaluate the relative importance of micropore and

macropore diffusions in the study of the adsorption kinetics by the DAB. If the value of γ is much greater than 1, the diffusion in zeolite pellet is controlled by the macropore diffusion. On the contrary, in the case of $\gamma \ll 1$, the diffusion approaches the micropore diffusion control. Both diffusion mechanisms are comparable if γ is close to 1.

Since the pressure in the DAB was increased from 0 atm to an arbitrary pressure, the zero coverage in the adsorbed phase was assumed as an initial condition. However, to apply NBDM to an experimental uptake obtained from the stepwise gravimetric method in this study, the Do's model should be modified to allow for non-zero coverage as an initial condition as follows:

Equation (7) was converted into the following equation:

$$\varepsilon \frac{\partial C_p}{\partial t} + (1-\varepsilon)\left(\frac{\partial \bar{C}_c}{\partial C_p}\right)\left(\frac{\partial C_p}{\partial t}\right) = \varepsilon D_p(T_p)\frac{1}{r_p^2}\frac{\partial}{\partial r_p}\left(r_p^2\frac{\partial C_p}{\partial r_p}\right) \quad (12)$$

Equation (12) was converted into the following form:

$$\frac{\partial C_p}{\partial t} = \frac{\varepsilon D_p(T_p)}{\varepsilon + (1-\varepsilon)(\partial \bar{C}_c/\partial C_p)}\frac{1}{r_p^2}\frac{\partial}{\partial r_p}\left(r_p^2\frac{\partial C_p}{\partial r_p}\right) = D_e(T_p)\frac{1}{r_p^2}\frac{\partial}{\partial r_p}\left(r_p^2\frac{\partial C_p}{\partial r_p}\right) \quad (13)$$

Because the equilibrium relation is assumed to be linear in the range of the pressure change, the slope of the isotherm in Eq. (13) was expressed as follows:

$$\left(\frac{\partial \bar{C}_c}{\partial C_p}\right)_{C_i \to C_e} = \frac{C_{ce} - C_{ci}}{C_{pe} - C_{pi}} \quad (14)$$

Since the mass balance equation derived for the diffusion in pellet, Eq. (13), was similar to that in crystal, Eq. (5), the following dimensionless form, γ, was applied to the criterion of the relative importance of macropore and micropore diffusions. The diffusion time constant, D/R^2, was used in order to neglect the effect of the diffusion length on the diffusion rate.

$$\gamma = \frac{\frac{D_{ci}}{R_c^2}}{\frac{\varepsilon D_{pi}}{(\varepsilon+(1-\varepsilon)(C_{ce}-C_{ci})/(C_{pe}-C_{pi}))R_p^2}} = \frac{D_{ci}/R_c^2}{\sigma_1 D_{pi}/R_p^2} = \frac{D_{ci}/R_c^2}{D_{ei}/R_p^2} \quad (15)$$

Dependence of Diffusivity on Concentration and Temperature

The dependence of micropore diffusion time constant on fractional coverage can be expressed by Darken equation with Langmuir and Langmuir-Freundlich (L-F) isotherms, respectively.

$$\frac{D_{ci}}{R_c^2} = \frac{D_{c0}}{R_c^2}\frac{1}{(1-\theta)}, \quad \theta = \frac{q}{q_s}, \quad q = \frac{q_s b P}{1+bP} \text{ Langmuir isotherm} \quad (16a)$$

$$\frac{D_{ci}}{R_c^2} = \frac{D_{c0}}{R_c^2}\frac{n}{(1-\theta)}, \quad \theta = \frac{q}{q_s}, \quad q = \frac{q_s b P^{1/n}}{1+bP^{1/n}} \text{ L-F isotherm} \quad (16b)$$

where θ is fractional coverage and D_{c0}/R_c^2 is corrected micropore diffusion time constant.

Also, effective macropore diffusivity, D_e, has the following relations with the macropore diffusivity, D_p.

$$D_e(T_p) = \frac{\varepsilon D_p(T_p)}{(\varepsilon + (1-\varepsilon)(C_{ce} - C_{ci})/(C_{pe} - C_{pi}))} = \sigma_1 D_p(T_p) \quad (17)$$

In the single component system, the macropore diffusion takes place by Knudsen diffusion and Poiseuille flow (Scott and Dullien, 1962; Kärger and Ruthven, 1992).

$$D_p(T_p) = \frac{1}{\tau}(D_K(T_p) + D_{\text{Poiseulle}}(T_p)) \quad (18)$$

where the Poiseuille diffusivity can be estimated by

$$D_{\text{Poiseuille}} = p_{\text{ave}}\gamma^2/8\eta \quad (19)$$

The p_{ave} in Eq. (19) means the average pressure of the initial and equilibrated pressure in each pressure step.

Since the micropore diffusivity depends on pressure according to Eq. (16), the corrected diffusion time constant, D_{c0}/R_c^2, was used in comparing among the diffusivities measured at different temperatures. The activation energy of micropore diffusion, E, can be derived from Eyring equation as follows:

$$\frac{D_{c0}}{R_c^2} = \frac{D_\infty}{R_c^2}\exp\left(\frac{-E}{RT}\right) \quad (20)$$

where D_∞/R_c^2 refers to the pre-exponential factor.

Experiment

The adsorbents used in the study were pelletized zeolite 4A and zeolite X type ion-exchanged by Ca which contains 11.51 wt% of CaO and 3.63 wt% of Na_2O. The detailed characteristics of the adsorbents are shown in Table 1. The adsorbate was CO_2 with higher than 99.99% purity.

The kinetics and equilibrium of adsorption were measured by the gravimetric method using electrobalance (Cahn, 2000). The adsorbents were thermally regenerated in a furnace at 513 K for 48 hours. About 50 mg of adsorbent was put into the basket in the hang-down tube of the electrobalance. The basket was made of aluminum mesh in order to make it easy to emit the heat of adsorption into the gas phase. The adsorbents in the container were regenerated for more than 7 hours at 513 K in vacuum conditions. The system was evacuated to the extent of less than 10^{-4} mmHg by the vacuum pump and diffusion pump before the experiment. A mercury manometer was used to measure the pressure of the adsorbate in the system. A circulating thermostat (Jeiotech Co., Rec-11) was set up in order to keep the temperature of the system constant.

Table 1. Characteristics of adsorbents.

Properties	Adsorbents		Unit
	Zeolite 4A	Zeolite CaX	
Producer	UOP Co.	Baylith (WE-G 639)	
Average pellet diameter	3.327	3.600	mm
Bulk density (ρ_B)	0.720	0.680	g/cm^3
Pellet density (ρ_P)	1.09	1.10	g/cm^3
Macropore porosity (ε_P)*	0.34	0.31	–
Average macropore diameter (d_P)*	2000	782	Å
Micropore diameter**	3.6–4.0	8.0–9.0	Å
Heat capacity (C_{ps})	0.84	0.92	J/g·K

*These values were obtained from mercury porosimeter.
**These values were obtained from Barrer (1978).

The adsorbate was supplied to the system by the fine valve within a short time (less than 0.5 second). The pressure of the adsorbate was increased in a stepwise manner from 0 atm to 0.8 atm and the uptake curve was measured at each pressure range as shown in Fig. 1. The step increase of the pressure in the system was

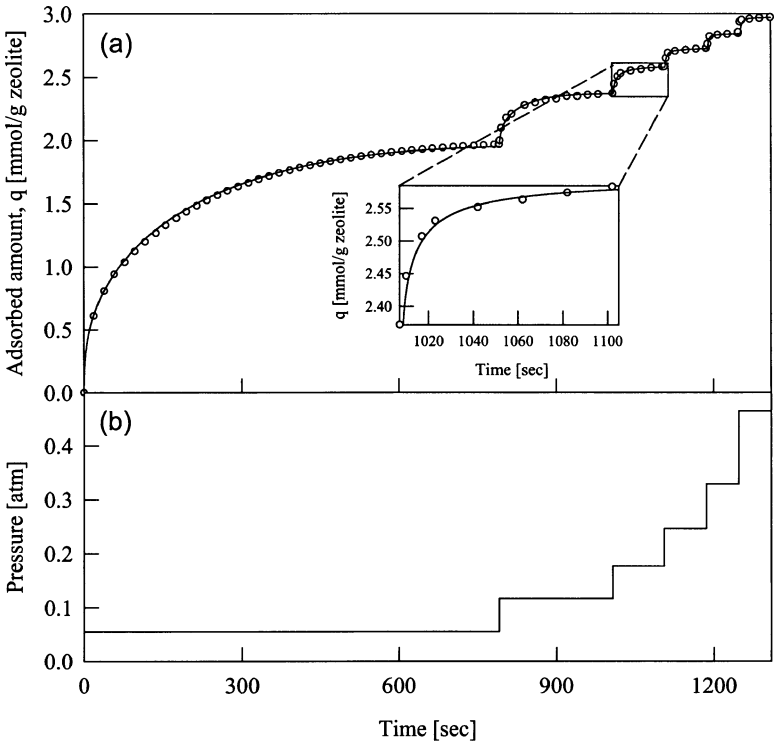

Figure 1. The measurement of the uptake curve by stepwise pressure increase in the gravimetric method.

sustained within the range of 50–60 mmHg to ensure the assumption that the equilibrium relation is linear within the pressure variation. In order to prevent the system from being contaminated by the pollutant, the system was rinsed with He for more than 2 hours after finishing each experiment.

Results and Discussions

Adsorption Equilibrium

In Fig. 2, the equilibrium isotherms of CO_2 in zeolite 4A and CaX pellets are shown in the range of 273–313 K and 0.0–0.8 atm. While the equilibrium isotherms of CO_2 in zeolite 4A pellet was well fitted by L-F isotherm, they showed a significant deviation from Langmuir isotherm in Fig. 2(a). This implies that the adsorption energy of CO_2 in zeolite 4A pellet is not uniform. However, the CO_2 adsorption in the zeolite CaX pellet was relatively well fitted by Langmuir isotherm as well as by L-F isotherm as shown in Fig. 2(b). The values of the isotherm parameters are listed in Table 2. As the parameter n in the L-F isotherm became greater, the isotherm became closer to irreversible isotherm type.

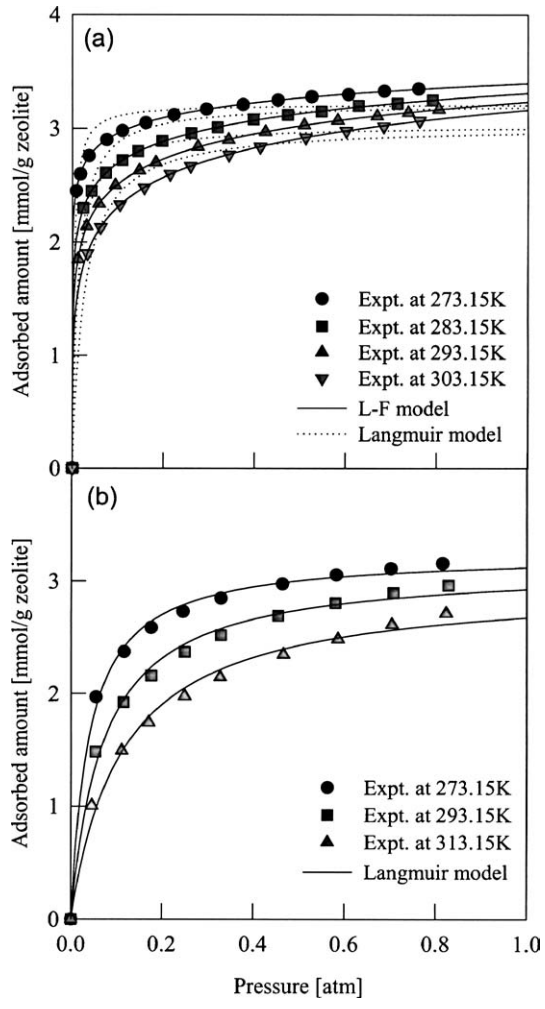

Figure 2. Equilibrium isotherms of CO_2 on (a) zeolite 4A and (b) zeolite CaX.

Table 2. Values of isotherm parameters at various temperatures.

Temp. (K)	q_s (mol/kg)	b (1/atm)	$1/n$ (−)
CO_2 in zeolite 4A—*Langmuir-Freudlich isotherm*			
273	5.059	2.043	0.162
283	5.051	1.901	0.221
293	5.041	1.790	0.257
303	5.020	1.703	0.301
CO_2 in zeolite CaX—*Langmuir isotherm*			
273	3.242	24.94	
293	3.129	14.16	
313	2.972	8.887	

The heat of adsorption for the CO_2/4A system was fixed to be 22 kJ/mol referring to the published ones (Yucel and Ruthven, 1980b; Haq and Ruthven, 1986a). In case of the CO_2/CaX system, the initial heat of adsorption was reported to be 50.5kJ/mol (Brandani et al., 2003). Therefore, it seems that the average heat of adsorption in the pressure range of 0.0–0.8atm should be a little lower than 50.5kJ/mol. In this study, we assumed that the heat of adsorption for the CO_2/CaX system would be 45 kJ/mol.

Controlling Mechanism of Diffusion Rate

The diffusion rate in the zeolite pellet was affected not only by micropore diffusion in the zeolite crystal but also by the diffusion in the macropore formed in pelletization. Since the size of the macropore is much greater than that of the micropore, the macropore diffusion is generally much faster than the micropore diffusion. However, since the radius of the crystal, that is the diffusion length of the crystal (R_c), is very short compared with that of the pellet (R_p), the difference in the diffusion length between crystal and pellet may be comparable to the difference of diffusivities of crystal

and pellet. As the crystal becomes smaller or the pellet becomes larger, the system increasingly approaches macropore diffusion control. Therefore, diffusion time constant (D/R^2) can be the rational criterion for estimating the relative importance of macropore and micropore diffusions (Ruthven and Xu, 1993; Ahn et al., 2002). Also, in the case of an irreversible or very strong favorable isotherm like the CO_2 isotherm in zeolites, a strong affinity between adsorbent and diffusing agent can make the macropore diffusion much slower at low pressure range. This can be explained by the increase of γ in Eq. (15).

In this study, the uptake curves for pellets of two different sizes were experimentally measured in the CO_2/4A and CO_2/CaX systems at the same temperature and pressure ranges. Then, the apparent diffusion time constant (D_a/R^2) was estimated by matching the experimental uptake curve to the analytical solution of NMDM. And the results were presented in Fig. 3.

While the diffusion length of micropore doesn't vary with the pellet size on the assumption that the average size of the zeolite crystal (R_c) in the pellet is constant, the diffusion length of macropore varies with the size of zeolite pellet (R_p). Therefore, if the micropore diffusion were the controlling step of overall diffusion rate, the diffusion time constants would not vary with the size change of the pellet. As shown in Fig. 3(a), the apparent diffusion time constants in the CO_2/4A system were constant regardless of the variation of the size of the pellet. The results indicated that the size of the pellet, that is the diffusion length of the pellet, did not have any effect on the overall diffusion rate. Therefore, the radius in the apparent diffusion time constant obtained from NMDM could be expected to be the radius of the crystal.

However, the CO_2/CaX system in Fig. 3(b) showed different tendency from the CO_2/4A system. The apparent diffusion time constant in a small pellet was greater than that in a large pellet. If the apparent diffusion time constant in the small pellet corresponded to that in the large pellet multiplied by the ratio of the square of the radius of each pellet, the dominant diffusion mechanism would be macropore diffusion and the radius in the apparent diffusion time constant obtained from NMDM would be the pellet radius. However, in the whole experimental range of pressure, the apparent diffusion time constants in the small pellet were not as great as the product of the apparent diffusion time constant in the large pellet and the ratio of square of the radius of each pellet. This means that both the macropore and micropore diffusions contributed to the overall diffusion rate in the CO_2/CaX system. In this case, the apparent diffusion time constant obtained from NMDM could not be defined by either the effective macropore or micropore diffusion time constant and it was only a lumped value showing the combined effect of the macropore and micropore diffusions. Therefore, in this case, the diffusivity should be estimated by nonisothermal bidisperse adsorption model (NBDM).

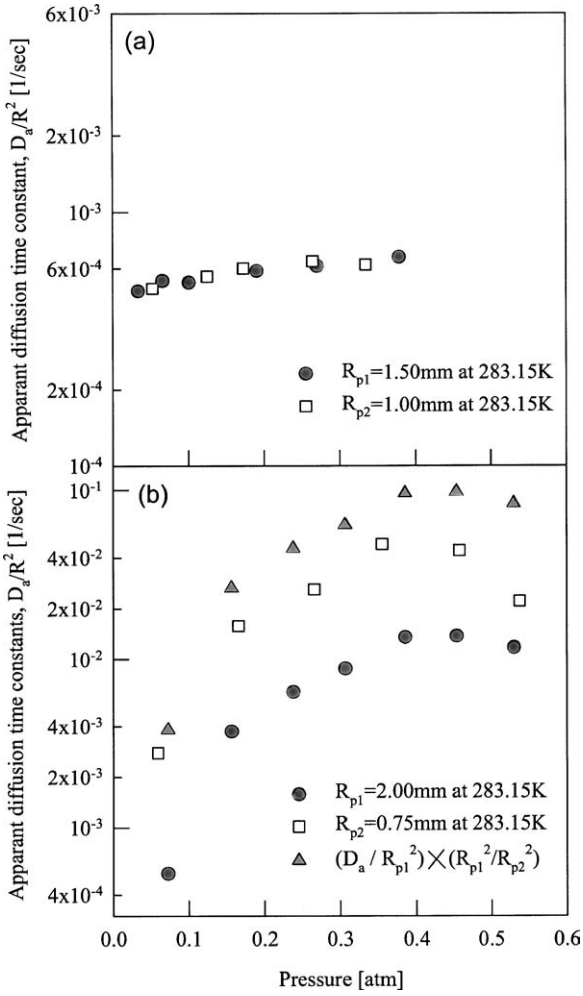

Figure 3. Comparison of apparent diffusion time constants for CO_2 diffusion in different size pellets at 283 K: (a) zeolite 4A and (b) zeolite CaX.

Diffusion Mechanism in CO_2/4A System

The representative uptake curves for the CO_2/4A system measured at two different pressure ranges are

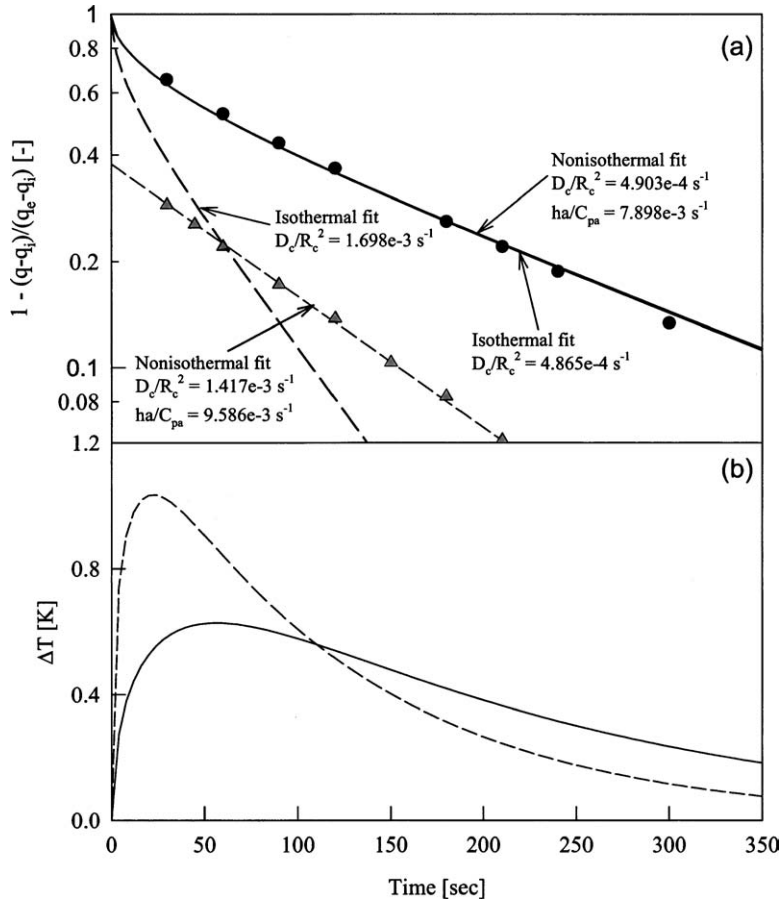

Figure 4. Comparing the simulations between nonisothermal model (NMDM) and isothermal model for the uptake curves of the CO_2/4A system.

presented in Fig. 4. As mentioned in Fig. 3, the nonisothermal monodisperse diffusion model (NMDM) was applied to the experimental data and its simulation result was compared with the result from the isothermal model. At low pressure range (0.0243–0.0421 atm), the prediction of isothermal model was in a good agreement with that of nonisothermal model. Therefore, at low pressure, the CO_2 molecules diffuse into the zeolite 4A pellet under the near-isothermal condition because the micropore diffusion time constant was very low although the adsorption amount was relatively large. However, at relatively high pressure range (0.513–0.602 atm) in Fig. 4(a), there was not a little difference between the predictions of nonisothermal and isothermal models. It means that as the micropore diffusion became faster with an increase of pressure, the dynamics of the CO_2 diffusion in the zeolite 4A pellet was close to nonisothermal behavior. Therefore, the temperature increase in the pellet was greater at the high pressure range (0.513–0.602 atm) than at the low pressure range (0.0243–0.0421 atm) in Fig. 4(b) although the change of adsorbed amount at the high pressure range was less than that at the low pressure range as shown in Fig. 2.

As a result, the dynamics of the CO_2 diffusion in the zeolite 4A pellet could be predicted not by an isothermal model but by the nonisothermal model like NMDM. However, it was reported that the CO_2 diffusion in zeolite 4A crystal bed showed an isothermal behavior but the CO_2 diffusion in zeolite 5A crystal bed was close to a nonisothermal behavior because the CO_2 diffusion in zeolite 4A crystal is slower than that in zeolite 5A crystal (Ruthven et al., 1980). This difference between this study and the reference can be explained in terms of the heat transfer parameter, ha/C_{ps}. The average value of $ha/C_{ps}\rho_p$ for the CO_2 diffusion in zeolite 4A pellet at each temperature are listed in

Table 3. Diffusional properties for micropore diffusion.

Temperature (K)	ave. ha/$C_{ps}\rho_p$ (1/sec)	D_{c0}/R_c^2 (1/sec)	D_∞/R_c^2 (1/sec)	E (kJ/mol)
	CO_2 in zeolite 4A			
273	7.721×10^{-3}	3.642×10^{-5}	1.892	24.57
283	7.812×10^{-3}	5.662×10^{-5}		
293	8.255×10^{-3}	7.940×10^{-5}		
303	8.964×10^{-3}	1.099×10^{-4}		

Temperature (K)	D_{c0}/R_c^2 (1/sec)	D_∞/R_c^2 (1/sec)	E (kJ/mol)
	CO_2 in zeolite CaX		
273	3.742×10^{-3}	4.097	15.97
293	5.672×10^{-3}		
313	8.936×10^{-3}		

Table 3 and they are kept constant to be the order of 10^{-3} s^{-1} in this study. However, the reported average value of $ha/C_{ps}\rho_p$ for the CO_2 diffusion in zeolite 4A crystal bed was in the order of 10^{-2} s^{-1} (Ruthven et al., 1980). It implies that it is more difficult to transfer the generated heat of adsorption to the surroundings in the zeolite pellet than in the crystal bed because the zeolite crystals are packed more densely in the pellet than in the crystal bed.

The corrected micropore diffusion time constant, D_{c0}/R_c^2, was obtained from each temperature. Figure 5

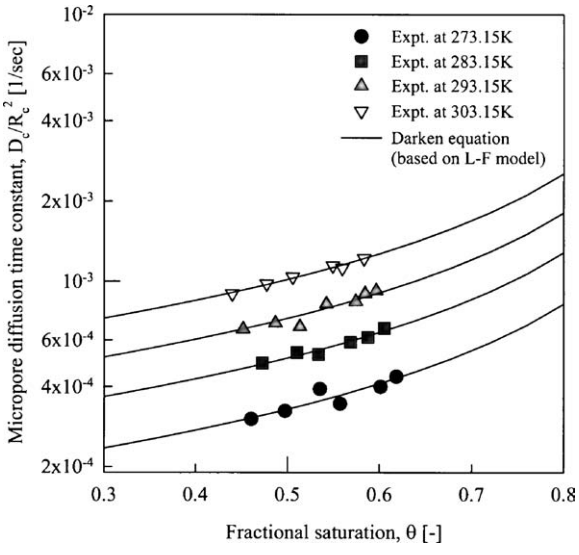

Figure 5. Coverage dependence of micropore diffusion time constants (D_c/R_c^2) for CO_2 diffusion in zeolite 4A.

compares the values of the micropore diffusion time constant estimated by NMDM with the result fitted by Darken equation, Eq. (16b), in the CO_2/4A system. As the uptake was measured at higher temperature, the micropore diffusion time constant clearly had an increasing tendency. Furthermore, since the equilibrium isotherm was highly favorable, the micropore diffusion time constant increased with an increase of fractional saturation or pressure according to Darken equation. The values of the corrected micropore diffusion constant at different temperatures are listed in Table 3.

Diffusion Mechanism in CO_2/CaX System

Figure 6 shows the uptake curves at different temperatures and low pressure in the CO_2/CaX system. A non-isothermal model considering dual diffusion should be applied to the analysis of the experimental uptake curve because both micropore and macropore diffusions contribute to the overall diffusion rate in the CO_2/CaX system as shown in Fig. 3. Therefore, the theoretical uptake curve and the corresponding temperature variation was simulated using NBDM. While the external heat transfer coefficient, h, in NMDM was estimated from the value of $ha/C_{ps}\rho_p$ by matching the experimental data to the mathematical model, the external heat transfer coefficient should be known as an input parameter in the NBDM. In general, the external heat transfer coefficient is assumed to be constant within the small ranges of pressure and temperature if the amount and the configuration of sample were not changed. Therefore, it was assumed that the value of the external heat transfer coefficient in the CO_2/CaX system would be nearly the same as that in the CO_2/4A system. The tortuosity factor of the zeolite CaX pellet was assumed to be 5 and the macropore diffusivity was estimated from the Knudsen diffusivity and Poiseuille flow according to Eq. (18). Therefore, in this system, the micropore diffusion time constant, D_c/R_c^2, the only unknown parameter, was estimated by matching the experimental uptake curves to NBDM.

Comparing the diffusion rates obtained at the condition of different temperature and similar pressure, the micropore and macropore diffusivities were larger at high temperature than at low temperature as shown in Fig. 6. Even if the macropore diffusivity did not show any significant variation in the narrow range of temperature, the effective macropore diffusivity, $D_e(=\sigma_1 D_p)$, would have a stronger dependency on the temperature

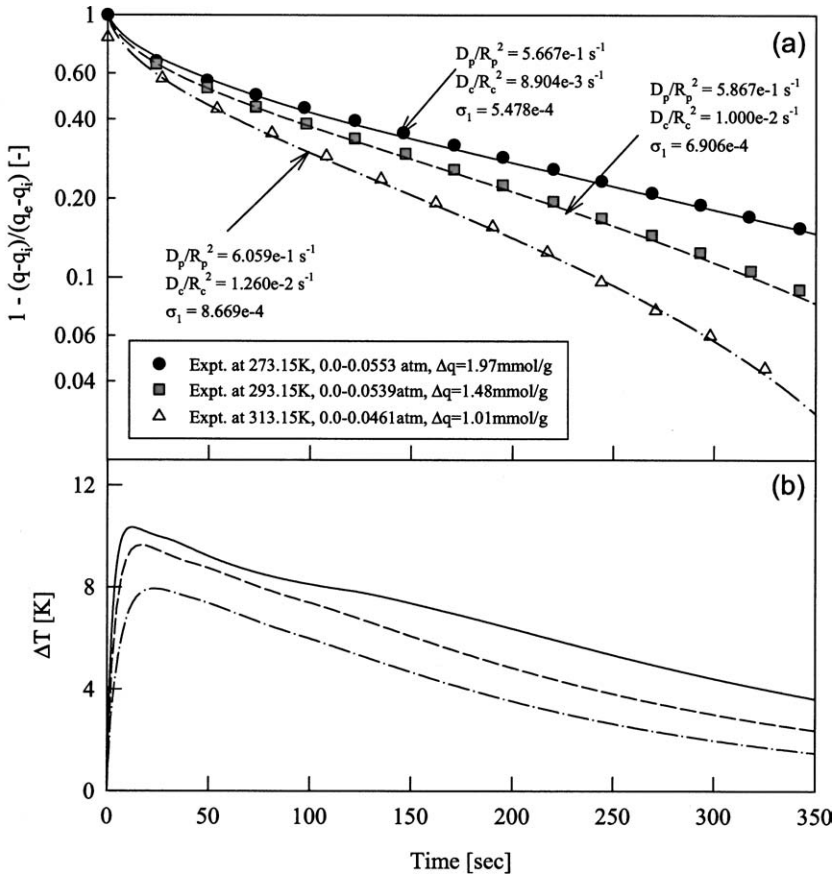

Figure 6. (a) Experimental uptake curves of CO_2 in zeolite CaX at different temperatures and similar pressure and the predicted transient uptake using NBDM and (b) the theoretical temperature profiles in solid phase.

than the macropore diffusivity due to some change of the slope of the isotherm with temperature.

Figure 7 shows the experimental uptake curves at different pressure ranges and 273 K in the CO_2/CaX system. Also, the theoretical uptake curves and the temperature variations predicted by NBDM were presented. While the macropore diffusivity did not show any significant variation with pressure, the values of σ_1 and D_e/R_p^2 increased steeply with an increase of pressure due to the strong favorable isotherm of the CO_2/CaX system. In addition, in the pressure range of over 0.5 atm, the fractional uptake showed an abrupt increase at the initial period, and then the diffusion rate mainly depended on the heat transfer rate from the adsorbent to the surroundings. The degree of the temperature increase in the pellet depended on the variation of the adsorbed amount rather than that of the diffusion rate as shown in Fig. 7(b). However, although the variation of the adsorbed amount at 0.0–0.055 atm was about 10 times greater than that at 0.117–0.176 atm, the temperature increase during the uptakes at 0.0–0.055 atm was less than 5 times greater than that at 0.117–0.176 atm. It implied that both macropore and micropore diffusion rates affected the temperature increase in the pellet to some extent.

Dimensionless Parameter, γ, in Controlling Mechanism of Diffusion Rate

The relative importance of the micropore and macropore diffusions in the CO_2/4A and CO_2/CaX systems was evaluated using the dimensionless parameter, γ, which was modified according to an initial condition of non-zero coverage in Eq. (15).

Figure 8 shows the variation of γ with pressure at different temperatures in the CO_2/4A system. The

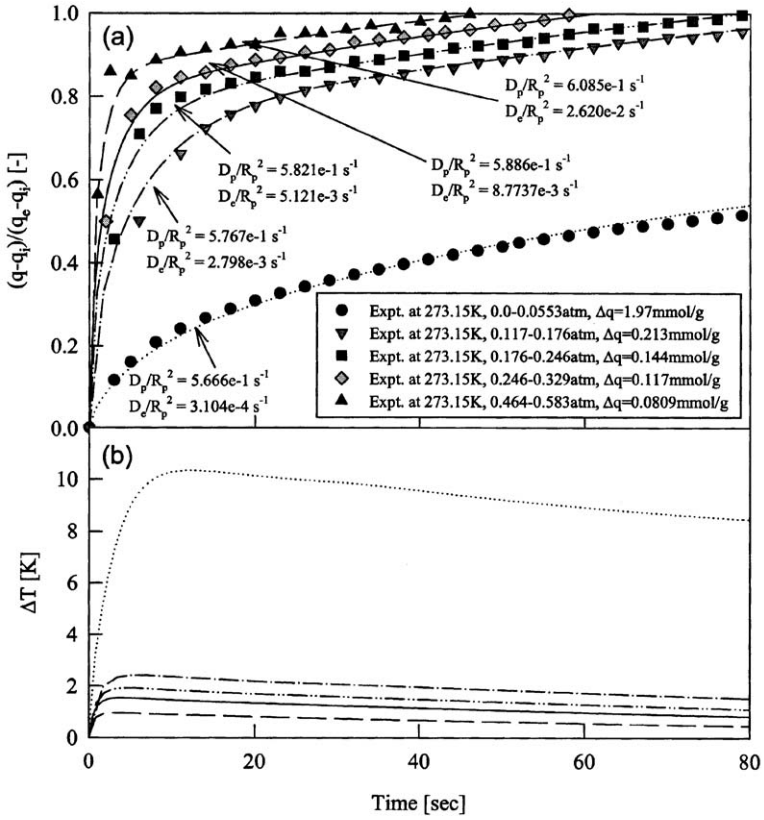

Figure 7. (a) Experimental uptake curves of CO_2 in zeolite CaX at different pressures and 273 K and the predicted transient uptake using NBDM and (b) the theoretical temperature profiles in solid phase.

macropore diffusivity was calculated assuming that the tortuosity of zeolite 4A pellet would be 4. When the value of γ is much less than unity, the micropore diffusion dominates the overall diffusion mechanism (Do, 1998). As the pressure increased, the value of γ decreased from about 0.1 at very low pressure to the order of 10^{-3} at about 0.8 atm as shown in Fig. 8. Judging from the result on the comparison of apparent diffusion time constants in pellets of two different sizes in Fig. 3(a), this range of γ implied micropore diffusion control.

As the pressure increased, the micropore diffusion time constant increased slightly according to Darken equation and the macropore diffusion time constant increased moderately due to the Poiseuille flow. However, σ_1 showed a steep increase with an increase of pressure, especially at the low pressure region, due to the very strong favorable isotherm of CO_2 adsorption in the zeolite 4A. Therefore, after the γ showed a steep decrease with an increase of pressure at the low pressure range, it decreased gradually with an increase of pressure. Also, the increase of γ with an increase of temperature could be explained by the decrease in the slope of the isotherm with temperature.

However, in Fig. 9, the σ_1 in the CO_2/CaX system increased smoothly with an increase of pressure compared with that in the CO_2/4A system. As a result, the decrease of γ with an increase of pressure in the CO_2/CaX system was smoother than that in the CO_2/4A system. The value of γ varied from a little higher than 10 at very low pressure to the order of 1 at about 0.8 atm. This range of γ indicated that both macropore and micropore diffusions contributed to the overall diffusion rate according to the result in Fig. 3(b). This result agreed well to Do's suggestion (1998) that $\gamma \approx 1$ meant the contribution of both diffusions.

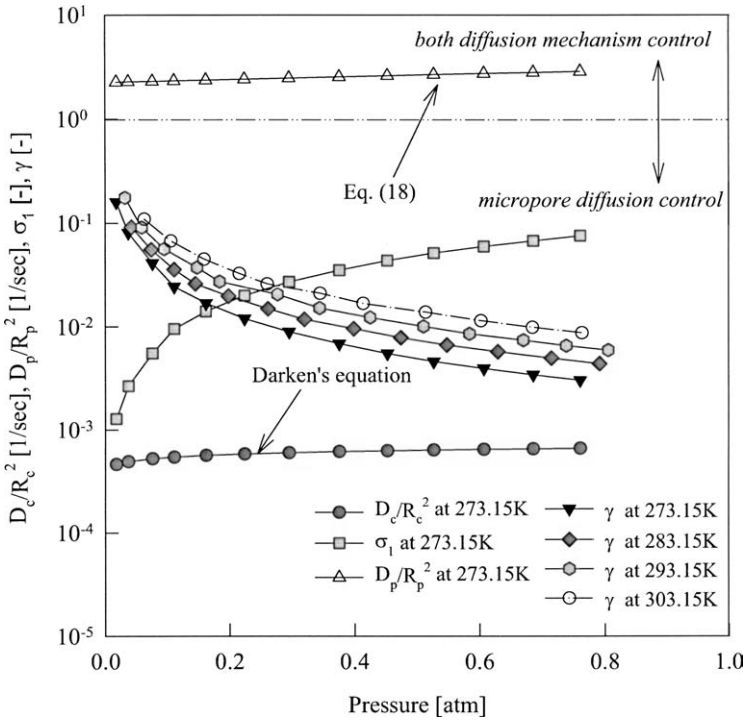

Figure 8. Pressure dependence of micropore diffusion time constant (D_c/R_c^2), effective macropore diffusion time constant (D_e/R_p^2), σ_1 and γ for CO_2 diffusion in zeolite 4A.

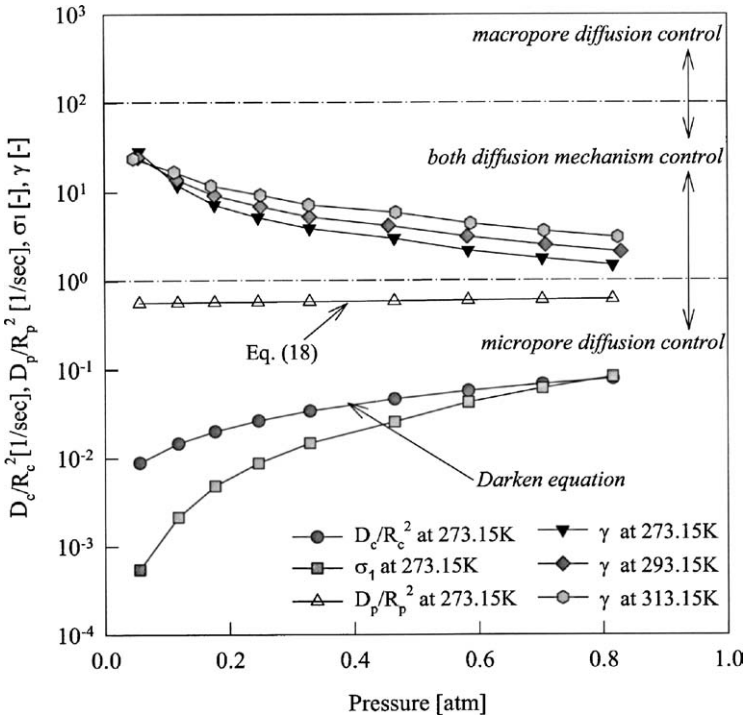

Figure 9. Pressure dependence of micropore diffusion time constant (D_c/R_c^2), effective macropore diffusion time constant (D_e/R_p^2), σ_1 and γ for CO_2 adsorption in zeolite CaX.

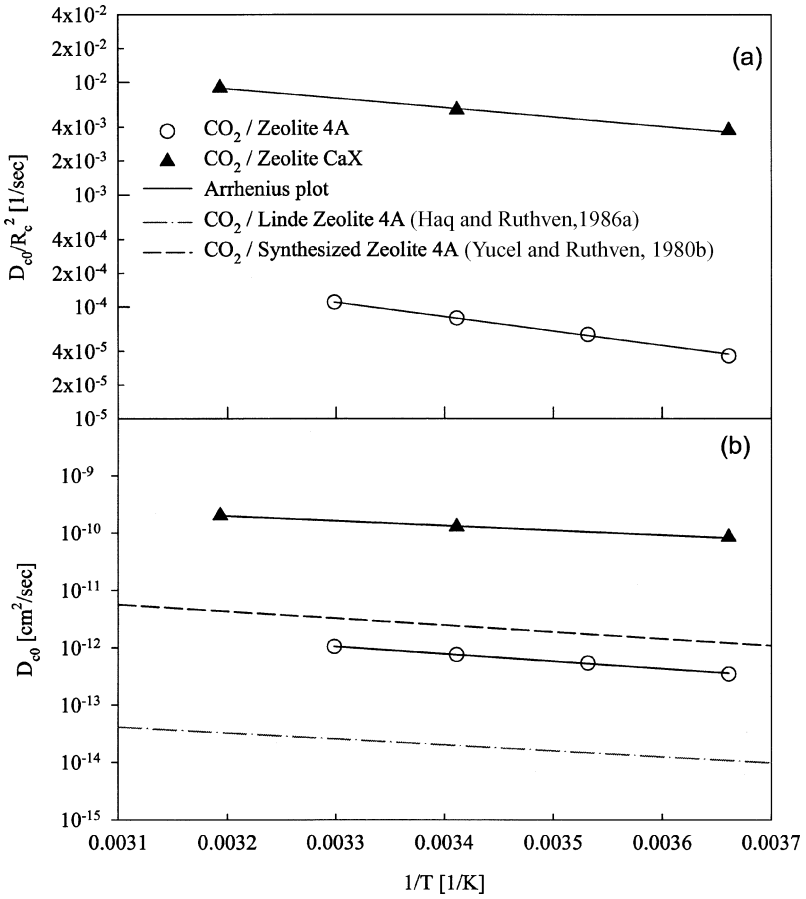

Figure 10. Temperature dependences of (a) corrected micropore diffusion time constant (D_{c0}/R_c^2) and (b) corrected micropore diffusivity (D_{c0}).

Activation Energy of Micropore Diffusion

Figure 10 shows Arrhenius plots for both the corrected micropore diffusion time constant and the micropore diffusivity obtained from Darken equation. The pre-exponential factor, D_∞/R_c^2, and the activation energy of micropore diffusion, E, were estimated from the Arrhenius plot in Fig. 10(a) and the values are listed in Table 3. The activation energy of the micropore diffusion was lower in the CO_2/CaX system than in the CO_2/4A system. This difference between the activation energies of two systems coincided with the result that the micropore diffusion rate in the CO_2/CaX system was faster than that in the CO_2/4A system. And the difference in the activation energy seemed to be associated with the difference of the micropore size of two adsorbents. Also, the activation energy in the CO_2/4A system was estimated to be similar to its heat of adsorption because the micropore diffusion played a key role in the overall diffusion mechanism in the CO_2/4A system.

The corrected micropore diffusivity was calculated from the corrected micropore diffusion time constant assuming the crystal radius of UOP 4A pellet would be approximately 1.95 μm (Ruthven, 2001). The corrected micropore diffusivity was in the order of 10^{-13} cm^2/s in the experimental range of temperature. In Fig. 10(b), the corrected micropore diffusivity of CO_2 on UOP 4A pellet was slightly less than that on Synthesized 4A crystal and greater than that on Linde 4A pellet (Yucel and Ruthven, 1980b; Haq and Ruthven, 1986a). Furthermore, the activation energy of CO_2 on UOP 4A pellet was estimated to be about 24.57 kJ/mol, which was very similar to 20.5 kJ/mol for Linde 4A pellet and 23 kJ/mol for Synthesized 4A crystal.

Conclusion

In this study, the diffusion mechanisms of CO_2 on commercial zeolite 4A and CaX pellets were theoretically and experimentally compared in the range of 0.0–0.8 atm and 273–313 K.

The apparent diffusion time constant was obtained by matching experimental uptake curve to nonisothermal monodisperse diffusion model (NMDM). However, it could not be determined to be either macropore or micropore diffusion before examining which diffusion mechanism dominates the overall diffusion rate. The dominant diffusion mechanism was determined by comparing the apparent diffusion time constants in pellets of two different sizes. Within the experimental pressure and temperature ranges in this study, the CO_2 diffusion in zeolite 4A pellet was controlled by the micropore diffusion and in case of the CO_2 diffusion in the zeolite CaX pellet, however, the overall diffusion rate was affected by both micropore and macropore diffusions. Therefore, the CO_2 diffusion in the zeolite CaX pellet should be studied using nonisothermal bidisperse diffusion model (NBDM) in which the coupled partial differential equations were numerically solved using the orthogonal collocation technique.

The micropore diffusion time constant in the CO_2/CaX system was approximately 100 times greater than that in the CO_2/4A system. Furthermore, the diffusion rates in the CO_2/4A and CO_2/CaX systems became faster with an increase of pressure owing to its strong favorable isotherm and they showed increasing tendency with an increase of temperature.

The modified dimensionless parameter, γ, considering non-zero coverage as an initial condition, gave the criterion for the relative importance of the micropore diffusion and the effective macropore diffusion in zeolite pellet. The dominant diffusion mechanism of overall diffusion rate could be determined according to the value of modified γ. γ over around 100 implies that macropore diffusion is dominant, and γ less than around 0.1 indicates the micropore diffusion control. In addition, γ between 100 and 0.1 is the realm in which both macropore and micropore diffusions contribute to overall diffusion rate. Finally, the activation energy of micropore diffusion was smaller in the CO_2/CaX system than in the CO_2/4A system because of the difference of micropore size of two adsorbents.

Appendix

The dimensionless variables and parameters were defined as

$$A_p = \frac{C_p - C_{pi}}{C_{pe} - C_{pi}}, \quad A_b = \frac{C_b - C_{pi}}{C_{pe} - C_{pi}}, \quad A_c = \frac{C_c - C_{ci}}{C_{ce} - C_{ci}}, \quad \bar{A}_c = \frac{\bar{C}_c - C_{ci}}{C_{ce} - C_{ci}} \tag{A1}$$

$$\theta_p = \frac{T_p - T_{pi}}{T_{pi}}, \quad x_p = \frac{r_p}{R_p}, \quad x_c = \frac{r_c}{R_c}, \quad \lambda = b_i C_{pi} \tag{A2}$$

$$\tau = \frac{(\varepsilon D_{pi})t}{(\varepsilon + (1-\varepsilon)(C_{ce} - C_{ci})/(C_{pe} - C_{pi}))R_p^2} \tag{A3}$$

$$\sigma_1 = \frac{\varepsilon}{(\varepsilon + (1-\varepsilon)(C_{ce} - C_{ci})/(C_{pe} - C_{pi}))} \tag{A4}$$

$$\sigma_2 = 1 - \sigma_1 \tag{A5}$$

$$\gamma = \frac{(\varepsilon + (1-\varepsilon)(C_{ce} - C_{ci})/(C_{pe} - C_{pi}))D_{ci}R_p^2}{\varepsilon D_{pi} R_c^2} = \frac{D_{ci}/R_c^2}{\sigma_1 D_{pi}/R_p^2} = \frac{D_{ci}/R_c^2}{D_{ei}/R_p^2} \tag{A6}$$

$$Bi = \frac{k_m R_p}{\varepsilon D_{pi}}, \quad LeBi_h = \frac{hR_p}{\rho_p C_{ps} D_{pi}} \tag{A7}$$

$$\psi = \frac{(1-\varepsilon)C_{ce}(-\Delta H)}{\rho_p C_{ps} T_{pi}}, \quad Q = \frac{D_p(T_p)}{D_{pi}} = (1+\theta_p)^{\beta} \tag{A8}$$

$$P = \frac{D_c(T_p)}{D_{ci}} = \exp\left(\frac{\alpha_c \theta_p}{1+\theta_p}\right); \quad \alpha_c = \frac{E}{RT_{pi}} \tag{A9}$$

$$B = \frac{b(T_p)}{b_i} = \exp\left(\frac{-\nu\theta_p}{1+\theta_p}\right); \quad \nu = \frac{(-\Delta H)}{RT_{pi}} \tag{A10}$$

Using the dimensionless groups and parameters, the mass balance in the crystal was converted into the following equation:

$$\frac{\partial A_c}{\partial \tau} = \gamma P \frac{1}{x_c^2} \frac{\partial}{\partial x_c}\left(x_c^2 \frac{\partial A_c}{\partial x_c}\right) \tag{A11}$$

with the following boundary conditions:

$$x_c = 0; \quad \frac{\partial A_c}{\partial x_c} = 0 \tag{A12}$$

$$x_c = 1; \quad A_c = \frac{(1+\lambda)BA_p}{(1+\lambda BA_p)} \tag{A13}$$

The mass balance in the pellet became

$$\sigma_1 \frac{\partial A_p}{\partial \tau} + \sigma_2 \frac{\partial \bar{A}_c}{\partial \tau} = Q \frac{1}{x_p^2} \frac{\partial}{\partial x_p} \left(x_p^2 \frac{\partial A_p}{\partial x_p} \right) \quad \text{(A14)}$$

with boundary conditions:

$$x_p = 0; \quad \frac{\partial A_p}{\partial x_p} = \frac{\partial \bar{A}_c}{\partial x_p} = 0 \quad \text{(A15)}$$

$$x_p = 1; \quad Q \frac{\partial A_p}{\partial x_p}\bigg|_1 = Bi(A_b - A_p|_1) \quad \text{(A16)}$$

and the heat balance in the pellet was reformed in the dimensionless form as follows:

$$\sigma_1 \frac{d\theta_p}{d\tau} + 3LeBi_h\theta_p - \sigma_1\psi(s+1) \times \int_0^1 \left(3\gamma P \frac{\partial A_c}{\partial x_c}\bigg|_1 \right) x_p^2 dx_p = 0 \quad \text{(A17)}$$

where the initial condition was

$$\tau = 0; \quad A_p = A_c = 0, \quad A_b = 1, \quad \theta_p = 0 \quad \text{(A18)}$$

Applying the $x_c^2 = u$ to Eq. (A11), it was converted into the following form:

$$\frac{\partial A_c}{\partial \tau} = 6\gamma P \frac{\partial A_c}{\partial u} + 4\gamma P u \frac{\partial^2 A_c}{\partial u^2} \quad \text{(A19)}$$

Equation (10) was changed into the following dimensionless form:

$$\bar{A}_c = \frac{3}{2} \int_0^1 u^{1/2} A_c du \quad \text{(A20)}$$

where one extra interpolation point was added (say, $u_{N+1} = 1$). Therefore, α and β in the Jacobi polynomial were determined to be 1 and 0.5, respectively. Also, the numbers of the collocation point (N) for the crystal and pellet were 5 and 11 except the boundary point. The collocation point was determined by the position on the x-axis where the Jacobi polynomial was zero. The Lagrange interpolation polynomial passing through all $(N+1)$ points was constructed as follows:

$$y_N(x) = \sum_{i=1}^{N+1} y_i l_i(x) \quad \text{(A21)}$$

The first and second derivatives of interpolation polynomial were expressed as follows:

$$y' = Am \cdot y, \quad y'' = \mathrm{Bm} \cdot y \quad \text{for crystal} \quad \text{(A22)}$$

$$y' = Ap \cdot y, \quad y'' = \mathrm{Bp} \cdot y \quad \text{for pellet} \quad \text{(A23)}$$

The mass balance in the crystal became:

$$\frac{\partial A_c(i)}{\partial \tau} = 6\gamma P \left(\sum_{j=1}^{5} Am(i,j)A_c(j) + Am(i,6)A_c(6) \right) + 4\gamma P u(i) \left(\sum_{j=1}^{5} Bm(i,j)A_c(j) + Bm(i,6)A_c(6) \right) \quad \text{for } i = 1, 2, \ldots, 5 \quad \text{(A24)}$$

where the boundary condition was

$$A_c(6) = \frac{(1+\lambda)BA_p}{1+\lambda BA_p} \quad \text{(A25)}$$

Similarly, applying $x_p^2 = \nu$ to Eq. (A14), the mass balance in the pellet became

$$\sigma_1 \frac{\partial A_p(i)}{\partial \tau} = 6Q \left(\sum_{j=1}^{11} Ap(i,j)A_p(j) + Ap(i,12)A_p(12) \right) + 4Q\nu(i) \left(\sum_{j=1}^{11} Bp(i,j)A_p(j) + Bp(i,12)A_p(12) \right) - 3\sigma_2\gamma P \sum_{j=1}^{6} Am(6,j)A_c(6) \quad \text{for } i = 1, 2, \ldots, 11 \quad \text{(A26)}$$

where the boundary condition was

$$A_p(12) = \frac{Bi(\nu(12) - \nu(11))A_b + 2QA_p(11)}{2Q + Bi(\nu(12) - \nu(11))} \quad \text{(A27)}$$

In summary, the coupled PDEs were reduced to sets of ODEs by the orthogonal collocation method. The resulting ODEs were integrated by the LSODE integration algorithm. The average values of transient concentration obtained at the collocation point in both crystal and pellet were calculated by the Radau quadrature.

Nomenclature

a	External surface area per unit volume of the zeolite pellet (1/cm)
b	Isotherm parameter (1/atm)
C_b	Bulk gas phase concentration (mol/kg)
C_c	Micropore concentration (mol/kg)
$\bar{C}_c$	Average concentration in the crystal (mol/kg)
C_p	Macropore concentration (mol/kg)
C_{ps}	Heat capacity of the zeolite (kJ/g·K)
D	Diffusivity (cm^2/sec)
D/R^2	Diffusion time constant (1/sec)
D_c	Micropore diffusivity (cm^2/sec)
D_{c0}/R_c^2	Corrected micropore diffusion time constant (1/sec)
D_e	Effective macropore diffusivity (cm^2/sec)
D_K	Knudsen diffusivity (cm^2/sec)
$D_{\text{Poiseulle}}$	Poiseuille diffusivity (cm^2/sec)
D_p	Macropore diffusivity (cm^2/sec)
D_∞/R_c^2	Pre-exponential factor (1/sec)
E	Activation energy of micropore diffusion (kJ/mol)
h	External film heat transfer coefficient (kJ/cm^2·sec·K)
K	Henry constant, –
K_0	Parameter in Eq. (20), –
k_m	External film mass transfer coefficient (cm/s)
M	Molecular weight (kg/mol)
n	Isotherm parameter, –
P	Pressure (atm)
q	Adsorbed amount (mol/kg)
q_s	Saturated adsorbed amount (mol/kg)
r_c	Radial distance of crystal (cm)
r_p	Radial distance of pellet (cm)
R	Gas constant (kJ/mol·K)
R_c	Crystal radius (cm)
R_p	Pellet radius (cm)
t	Time (sec)
T_p	Pellet temperature (K)
$-\triangle H$	Isosteric heat of adsorption (kJ/mol)

Greek Letters

α	Dimensionless parameter defined by Eq. (4), –
β	Dimensionless parameter defined by Eq. (4). –
ε	Macropore porosity, –
γ	Macropore diameter (cm)
η	Gas viscosity (atm·sec)
θ	Fractional coverage, –
ρ_p	Pellet density (g/cm^3)
τ	Tortuosity factor, –

Subscripts

e	Equilibrium state
i	Initial state

Acknowledgment

Financial assistance and support from KOSEF (R01-1999-000-00198-0) are gratefully acknowledged.

References

Ahn, H., H.-K. Yoo, Y. Shul, S. Hyun, and C.-H. Lee, "Diffusion Mechanism of N_2 and CH_4 in Pelletized Zeolite 4A, 5A and CaX," *J. Chem. Eng. Japan*, **35**(4), 334–345 (2002).

Barrer, R.M., *Zeolite and Clay Minerals as Sorbents and Molecular Sieves*, 1st edition, Academic Press, New York, 1978.

Brandani, F., D. Ruthven, and C.G. Coe, "Measurement of Adsorption Equilibrium by the Zero Length Column (ZLC) Technique Part I: Single-Component Systems," *Ind. Eng. Chem. Res.*, **42**, 1451–1461 (2003).

Brandani, S., "Analytical Solution for ZLC Desorption Curves with Bi-porous Adsorbent Particles," *Chem. Eng. Sci.*, **51**(12), 3283–3288 (1996).

Da Silva, F.A. and A.E. Rodrigues, "Adsorption Equilibria and Kinetics for Propylene and Propane over 13X and 4A Zeolite Pellets," *Ind. Eng. Chem. Res*., **38**, 2051–2057 (1999).

Do, D.D., *Adsorption Analysis: Equilibria and Kinetics,* Imperial College Press, London, UK, 1998.

Gray, P.G. and D.D. Do, "Dynamics of Carbon Dioxide Sorption on Activated-Carbon Particles," *AIChE J.*, **37**(7), 1027–1034 (1991).

Haq, N. and D.M. Ruthven, "Chromatographic Study of Sorption and Diffusion in 4A Zeolite," *J. Colloid Int. Sci.,* **112**, 154–163 (1986a).

Haq, N. and D.M. Ruthven, "Chromatographic Study of Sorption and Diffusion in 5A Zeolite," *J. Colloid Int. Sci.*, **112**, 164–169 (1986b)

Kärger, J. and D.M. Ruthven, *Diffusion in Zeolites and Other Microporous Solids*, Chap 4, John Wiley & Sons, Singapore, 1992.

Ma, Y.H. and C. Mancel, "Diffusion Studies of CO_2, NO, NO_2 and SO_2 on Molecular Sieve Zeolites by Gas Chromatography," *AIChE J.*, **18**(6), 1148–1153 (1972).

Ruthven, D.M., "Diffusion of Xe and CO_2 in 5A Zeolite Crystals," *Zeolites*, **13**, 594 (1993).

Ruthven, D.M., "Short Communication: Diffusion of Simple Molecules in 4A Zeolite," *Adsorption*, **7**, 301–304 (2001).

Ruthven, D.M., L.K. Lee, and H. Yucel, "Kinetics of Non-isothermal Sorption in Molecular Sieve Crystals," *AIChE J.*, **26**, 16–23 (1980).

Ruthven, D.M., and Z. Xu, "Diffusion of Oxygen and Nitrogen in 5A Zeolite Crystals and Commercial 5A Pellets," *Chem. Eng. Sci*., **48**, 3307–3312 (1993).

Scott, D.S. and F.A.L. Dullien, "Diffusion of Ideal Gases in Capillaries and Porous Solids," *AIChE J.*, **8**(1), 113–117 (1962).

Silva J.A.C. and A.E. Rodrigues, "Analysis of ZLC Technique for Diffusivity Measurements in Bidisperse Porous Adsorbent Pellets," *Gas. Sep. Purif.*, **10**(4), 207–224 (1996).

Silva J.A.C. and A.E. Rodrigues, "Sorption and Diffusion of n-Pentane in Pellets of 5A Zeolite," *Ind. Eng. Chem. Res.*, **36**, 493–500 (1997).

Silva J.A.C., F.A. Da Silva, and A.E. Rodrigues, " An Analytical Solution for the Zero-Length-Column Experiments with Heat Effects," *Ind. Eng. Chem. Res.*, **40**, 3697–3702 (2001).

Wakao, N. and S. Kaguei, *Heat and Mass Transfer in Packed Beds,* Gordon and Breach, New York, 1982.

Yucel, H. and D.M. Ruthven, "Diffusion in 4A Zeolite: Study of the Effect of Crystal Size," *J. Chem. Soc. Faraday Trans. I*, **76**, 60–70 (1980a).

Yucel, H. and D.M. Ruthven, "Diffusion of CO_2 in 4A and 5A Zeolite Crystals," *J. Colloid Int. Sci.*, **74**, 186–195 (1980b).